Progress In Electromagnetics Research C, Vol. 127, 17–29, 2022

Speed Sensorless Control of Bearingless Synchronous Reluctance Slice Motor Considering the Effect of Suspension Force Windings

Ruichen Li and Huangqiu Zhu*

Abstract—In this paper, the effect caused by the suspension force windings on the torque windings in a bearingless synchronous reluctance slice motor (BsynRSM) is analyzed, and a new slide model observer is proposed to reduce the speed estimation vibration caused by this effect. Firstly, the effect of suspension force windings is analyzed in a Maxwell model. The suspension force windings will generate an asynchronous torque and current, which are similar to superimposing an asynchronous motor on the original motor. And a special Matlab/Simulink model is built. Secondly, the effect of current and torque generated by suspension force windings on speed sensorless is analyzed. The sliding mode observer (SMO) is studied considering the effect of suspension force windings. Simulation result shows that the current generated by suspension force windings of the BsynRSM will cause the estimate speed vibrating with the rotor vibration, and the frequency of speed estimation vibration is much higher than the additional current and torque generated by the suspension force windings. Thirdly, an improved SMO is proposed. By using the improved SMO, the amplitude and frequency of the speed estimation are obviously reduced. Finally, the improved SMO is verified on the experimental platform, which proves the feasibility of the method.

1. INTRODUCTION

As a new type of motor, bearingless motor has a combined winding or separate winding placed in the stator, and the rotor is stably suspended in the center position by controlling the windings current. It has outstanding advantages such as no friction, high speed, high precision, and maintenance-free [1, 2].

Bearingless slice motor is a special bearingless motor structure whose rotor length is much smaller than diameter. Bearingless slice motor has the advantage that the rotor can be easily isolated from the stator. Therefore, it is very suitable for using in special occasions such as strong corrosion and high radioactivity [3–5]. Usually, the bearingless slice motor adopts a permanent magnet rotor. However, with the increase of the international permanent magnet price, the motor using a large number of permanent magnets is obviously uneconomical.

Bearingless synchronous reluctance motor (BsynRM) is an excellent alternative to bearingless permanent magnet motor. It has low loss and strong robustness without using expensive permanent magnets. Compared with induction motors, it has better performance [6–8]. In recent years, with the research on the efficiency and torque ripple of BsynRM, BsynRM has further developments [9, 10].

Bearingless synchronous reluctance slice motor (BsynRSM) combines a BsynRM with a slice rotor. BsynRM can realize three degrees of freedom passive suspension like bearingless permanent magnet slice motor (BPMSM), when the motor torque magnetic field is constructed. The rotor of BsynRSM does not need permanent magnets, which effectively reduces the manufacturing cost and maintenance cost of the rotor. There is a few researches on the BsynRSM in recent years [11–13].

Received 11 October 2022, Accepted 12 November 2022, Scheduled 21 November 2022
* Corresponding author: Huangqiu Zhu (zhuhuangqiu@ujs.edu.cn).
The authors are with the School of Electrical and Information Engineering, Jiangsu University, Zhenjiang 212013, China.

The special structure of a bearingless slice motor without a rotating shaft means that it cannot use a photoelectric encoder for speed measurement. Usually, bearingless slice motors use Hall sensors to measure rotor position. However, Hall sensors are greatly disturbed by temperature and external magnetic field, and the installation is complicated. Hall sensors also require additional control modules. Therefore, the research on sensorless technology will effectively improve the performance of bearingless motors.

Existing research on speed sensorless control is based on torque windings, and BsynRSM is analogous to common synchronous reluctance motor. So, the effect of suspension force windings on the torque windings is not considered. However, the suspension force windings of BsynRSM will undoubtedly have an impact on the magnetic field of the motor, and it will also have a certain impact on the speed sensorless control performance.

In this paper, it is firstly verified that the conclusion of the effect of the suspension force windings on torque windings of the BsynRM can be applied to the BsynRSM. After that, a new BsynRSM model was constructed in Matlab/Simulink, and this model is used to analyze the effect of the suspension force windings on the traditional sliding model observer (SMO). Then an improved SMO is proposed to reduce the adverse effect caused by suspension force windings. Finally, the performance of the improved SMO is verified by the simulation results, and it is verified on the experimental platform. The results show that the proposed improved SMO can effectively reduce the vibration caused by the suspension force windings.

2. OPERATION PRINCIPLE AND MATHEMATICAL MODELS OF BSYNRSM

In BsynRSM, the suspension force windings and torque windings are placed in the stator, and the torque winding will generate torque. The suspension force windings generate suspension magnetic field, which is superposed with the magnetic field of the torque winding to keep the rotor stably suspended. Based on the basic suspension conclusion, the pole pair of torque winding $P_M = 1$, and the pole pair of levitation winding $P_B = 2$. In addition, two basic conditions need to be satisfied: the electromagnetic frequencies of two windings are equal ($\omega_1 = \omega_2$), and the rotating magnetic fields are in the same direction.

2.1. Operation Principle of Active Suspension Force

As shown in Figure 1, when the two sets of windings are fed of current, they will generate 4-pole magnetic flux and 2-pole magnetic flux, respectively. When the magnetic fields generated by the two

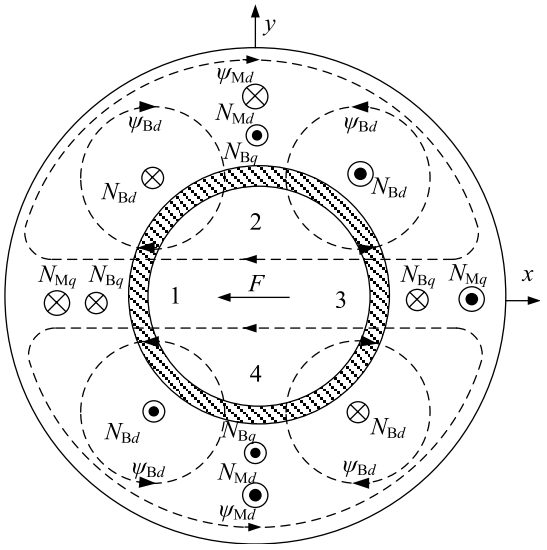

Figure 1. Generation principle of active suspension force.

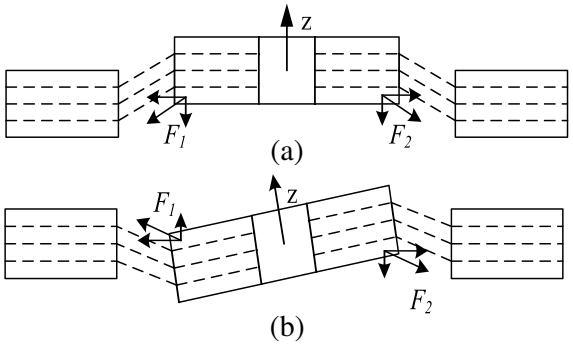

Figure 2. Generation principle of passive suspension force.

sets of windings are superimposed, the magnetic field at air gap 1 is strengthened, and the magnetic field at air gap 3 is weakened. So, a suspension force along the negative direction of the x-axis of the magnetic field increases. By changing the direction of the current vector, the direction of the suspension force can be controlled. As the active suspension force is generated by the superposition of the suspension force winding and torque winding, obviously the suspension force winding will have a certain effect on the torque magnetic field.

2.2. Operation Principle of Passive Stabilization

Compared with the traditional bearingless motor, the biggest advantage of the bearingless slice motor is that it can realize three degrees of freedom passive suspension. Although the rotor of the BsynRSM does not contain permanent magnets, its passive suspension principle is similar to a permanent magnet rotor. When the magnetic field of the torque winding is established, as shown in Figure 2, according to the principle of minimum reluctance, when the rotor is located at the center of the stator, the magnetic flux path is the shortest. So it can be stabilized at the center position. When the disturbance causes the rotor to deviate from the center, the rotor is subjected to an electromagnetic force opposite to the disturbance force, pulling the rotor back to the center position.

2.3. Mathematical Model of the BsynRSM

The mathematical model of a BsynRSM is similar to that of a BsynRM. Based on the Maxwell tensor method, the Maxwell force on the rotor and the controllable suspension force generated by the suspension force winding can be obtained. Due to the passive suspension characteristics of the slice motor, it is unnecessary to consider the effect of rotor gravity. The controllable suspension force needs to balance the Maxwell force and disturbance force on the rotor to ensure the stable suspension of the rotor [14]

$$\begin{cases} -F_x + F_{sx} + F_{zx} = 0 \\ -F_y + F_{sy} + F_{zy} = 0 \end{cases} \tag{1}$$

where F_x, F_y are controllable suspension forces in x-direction and y-direction; F_{sx}, F_{sy} are Maxwell forces; F_{zx}, F_{zy} are the disturbance forces on the rotor.

The Maxwell force on the rotor is

$$\begin{bmatrix} F_{sx} \\ F_{sy} \end{bmatrix} = \frac{k\pi r l B^2}{\mu_0 \delta_0} \begin{bmatrix} x \\ y \end{bmatrix} = K_s \begin{bmatrix} x \\ y \end{bmatrix} \tag{2}$$

where k is the proportional coefficient related to motor structure, r the rotor salient radius, l the effective iron core length of the motor, B the field strength, μ_0 the vacuum permeability, and δ_0 average length of air gap

The controllable suspension force is

$$\begin{bmatrix} F_x \\ F_y \end{bmatrix} = \begin{bmatrix} K_{m1} i_{dM} & K_{m2} i_{qM} \\ K_{m2} i_{qM} & -K_{m1} i_{dM} \end{bmatrix} \begin{bmatrix} i_{dB} \\ i_{qB} \end{bmatrix} \tag{3}$$

where $K_{m1} = \frac{lr\mu_0 N_1 N_2}{48\delta_0^2}(2\pi + 3\sqrt{3})$, $K_{m2} = \frac{lr\mu_0 N_1 N_2}{48\delta_0^2}(2\pi - 3\sqrt{3})$, N_1 is the effective turns in series of each phase of torque windings; N_2 is the effective turns in series of each phase of suspension windings i_{dM}, i_{qM} are the torque winding currents in d-direction and q-direction; i_{dB}, i_{qB} are the suspension winding currents in d-direction and q-direction.

Based on the model of BsynRM, the torque model of BsynRSM can be obtained

$$T_e = \frac{3}{2} P_M (L_d - L_q) i_{dM} i_{qM} \tag{4}$$

where i_{dM}, i_{qM} are the motor inductances in d-direction and q-direction.

3. EFFECT OF SUSPENSION FORCE WINDINGS ON TORQUE WINDINGS

According to the active and passive suspension principle of BsynRSM, when the motor runs stably, the suspension force winding will generate magnetic field, which will break the balance of the torque windings to provide suspension force. In previous studies, the effect of suspension force windings on torque windings is usually ignored in order to reduce the complexity of the system. However, suspension force windings may generate additional torque, which will affect the accuracy of the speed sensorless control. This effect will also increase the vibration of the speed estimation and reduce the stability of the system operation. According to previous research on BsynRM, suspension force windings may generate additional torque to the torque winding, and it may lead to additional eddy current loss and hysteresis loss [15].

A Maxwell model is built to find the effect of the suspension winding on torque winding in BsynRSM based on the conclusion of BsynRM. The parameters of the BsynRSM model is in Table 1. Due to the structural characteristics of the slice motor, it does not need to overcome the gravity during normal operation. So the suspension force winding current of a BsynRSM is smaller than that of a BsynRM. And the suspension force winding current during normal operation is much smaller than the current

Table 1. Parameters of BsynRSM.

Parameter (Unit)		Value
Rated voltage	U (V)	220
Rated power	P (kW)	4
Rated speed	n (r/min)	3000
Number of phases	m	3
Breath length	l (mm)	2
Outer diameter of rotor	D_{r1} (mm)	80
Turns of torque winding	W_1 (n)	100
Turns of suspension force winding	W_2 (n)	100
Pole number of slice rotor	P_{PM}	4
Pole number of torque winding	P_M	4
Pole number of suspension force winding	P_B	2

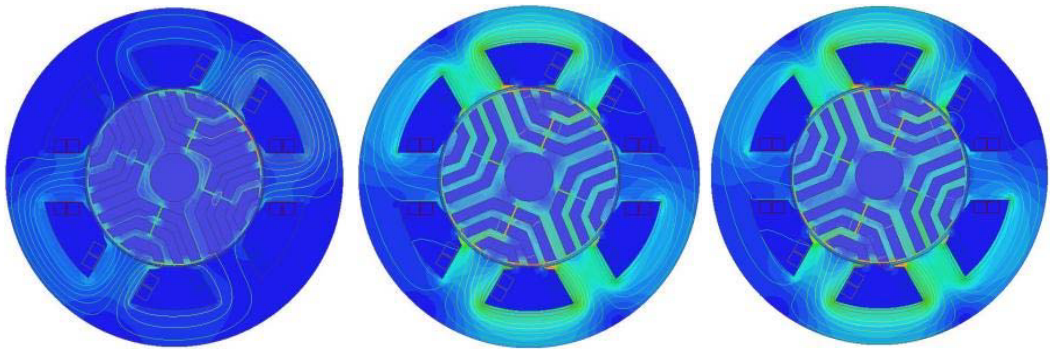

Figure 3. Maxwell simulation of motor magnetic field, (a) only suspension force winding is active, (b) only torque winding is active, (c) both suspension force winding and torque winding are active (the computational mesh of the rotor and the stator is 5 mm, and the computational mesh of the motor is 10 mm).

when the motor stars. To ensure that the superimposed magnetic field generated by the suspension force windings will not cause strong saturation under any operation conditions, the current of the suspension force windings during the simulation is set at the maximum. In this way, the effect of the suspension force windings on the magnetic field of the motor can be better seen. From Figure 1, when the motor operates normally, the magnetic field of the BsynRSM is equivalent to the superposition of the magnetic field generated by the suspension force windings and torque windings. As shown in Figure 3, the additional magnetic field generated by the suspension force windings has little effect on the motor saturation. Therefore, the suspension force magnetic field and torque magnetic field meet the superposition law. Thus, the asynchronous magnetic field model can be approximately equivalent to an asynchronous motor. The driving current of this motor is suspension force winding current, and the speed of this motor is the rotor speed. The asynchronous motor can generate additional torque and additional current. This torque and current can be directly added to the original motor. This equivalent asynchronous motor will also generate eddy current losses and hysteresis losses.

4. DESIGN AND IMPROVEMENT OF SLIDE MODEL OBSERVER

4.1. Traditional Slide Model Observer

The slide model observer (SMO) is a classic sensorless control strategy, which belongs to nonlinear control. SMO does not require high system model accuracy and is insensitive to parameter changes and external disturbances [16, 17]. Therefore, it has the advantages of strong robustness and simple design.

The SMO design is mostly based on the static coordinate system, so the motor voltage equation is written as:

$$\begin{bmatrix} u_\alpha \\ u_\beta \end{bmatrix} = \begin{bmatrix} R + \dfrac{\mathrm{d}}{\mathrm{d}t}L_d & \omega_e\left(L_d - L_q\right) \\ -\omega_e\left(L_d - L_q\right) & R + \dfrac{\mathrm{d}}{\mathrm{d}t}L_q \end{bmatrix} \begin{bmatrix} i_a \\ i_\beta \end{bmatrix} + \begin{bmatrix} E_a \\ E_\beta \end{bmatrix} \tag{5}$$

where R is the torque winding resistance; L_d, L_q are the stator inductances; ω_e is the electrical angular velocity; $\begin{bmatrix} u_\alpha & u_\beta \end{bmatrix}^T$ is the stator voltage; $\begin{bmatrix} i_\alpha & i_\beta \end{bmatrix}^T$ is the stator current; and $\begin{bmatrix} E_\alpha & E_\beta \end{bmatrix}^T$ is the extended back electromotive force (EMF).

For bearingless synchronous reluctance slice motors, EMF contains all information related to the rotor position and speed. Therefore, the more accurately the EMF of the motor is obtained, the more accurately the rotor position and rotational speed can be obtained. Changing the voltage equation to the current equation makes it easier to use SMO to observe the EMF, so rewrite (1)

$$\frac{\mathrm{d}}{\mathrm{d}t}\begin{bmatrix} i_\alpha \\ i_\beta \end{bmatrix} = \mathrm{A}\begin{bmatrix} i_\alpha \\ i_\beta \end{bmatrix} + \frac{1}{L_d}\begin{bmatrix} u_\alpha \\ u_\beta \end{bmatrix} - \frac{1}{L_d}\begin{bmatrix} E_\alpha \\ E_\beta \end{bmatrix} \tag{6}$$

where

$$\mathbf{A} = \frac{1}{L_d}\begin{bmatrix} -R & -\left(L_d - L_q\right)\omega_e \\ \left(L_d - L_q\right)\omega_e & -R \end{bmatrix} \tag{7}$$

To obtain EMF estimates, the SMO is designed as follows:

$$\frac{\mathrm{d}}{\mathrm{d}t}\begin{bmatrix} i_\alpha^{'} \\ i_\beta^{'} \end{bmatrix} = \mathbf{A}\begin{bmatrix} i_\alpha^{'} \\ i_\beta^{'} \end{bmatrix} + \frac{1}{L_d}\begin{bmatrix} u_\alpha \\ u_\beta \end{bmatrix} - \frac{1}{L_d}\begin{bmatrix} \nu_\alpha \\ \nu_\beta \end{bmatrix} \tag{8}$$

where $i_\alpha^{'}$, $i_\beta^{'}$ are the observed values of the stator current, and u_α, u_β are the observer control input.

So the stator current error equation is:

$$\frac{\mathrm{d}}{\mathrm{d}t}\begin{bmatrix} \tilde{i}_\alpha \\ \tilde{i}_\beta \end{bmatrix} = \mathbf{A}\begin{bmatrix} \tilde{i}_\alpha \\ \tilde{i}_\beta \end{bmatrix} + \frac{1}{L_d}\begin{bmatrix} E_\alpha - \nu_\alpha \\ E_\beta - \nu_\beta \end{bmatrix} \tag{9}$$

where $\tilde{i}_\alpha = i_\alpha^{'} - i_\alpha$, $\tilde{i}_\beta = i_\beta^{'} - i_\beta$ is the current observation error.

The slide model control law is designed as follows:

$$\begin{bmatrix} \nu_\alpha \\ \nu_\beta \end{bmatrix} = \begin{bmatrix} k\,\mathrm{sgn}\left(i'_\alpha - i_\alpha\right) \\ k\,\mathrm{sgn}\left(i'_\beta - i_\beta\right) \end{bmatrix} \tag{10}$$

where $k > \max\{-R\left|\tilde{i}_\alpha\right| + E_\alpha\,\mathrm{sgn}(\tilde{i}_\alpha), -R\left|\tilde{i}_\beta\right| + E_\beta\,\mathrm{sgn}(\tilde{i}_\beta)\}$.

When the state variable of the observer reaches the sliding surface $\tilde{i}_\alpha = 0$, $\tilde{i}_\beta = 0$

$$\begin{bmatrix} E_\alpha \\ E_\beta \end{bmatrix} = \begin{bmatrix} \nu_\alpha \\ \nu_\beta \end{bmatrix}_{eq} = \begin{bmatrix} k & \mathrm{sgn}\left(\tilde{i}_\alpha\right)_{eq} \\ k & \mathrm{sgn}\left(\tilde{i}_\beta\right)_{eq} \end{bmatrix} \tag{11}$$

Use the arctangent function to extract the signal

$$\theta'_{eq} = -\arctan\left(E'_a / E'_\beta\right) \tag{12}$$

The rotor position and speed information can be obtained.

4.2. Improved Slide Model Observer

When the effect of the suspension force windings on the torque windings is considered, the suspension force windings will generate additional current, and this additional current will adversely affect the EMF measurement of the motor. As the accuracy of the EMF measurement decreases, high frequency vibrations are also generated in the speed estimation. This high frequency vibration will reduce the stability of the motor operation and increase the radial vibration of the rotor.

Since sliding mode control is a discontinuous control method, the additional current causes more frequent vibration in the switching function used by the SMO. On the other hand, the phase lag of the EMF caused by the filter will further cause the error of the speed estimation.

In this paper, a new SMO is established by using the hyperbolic tangent curve instead of the switching function. Compared with the switching function, the hyperbolic tangent function does not jump at the zero point, which effectively reduces the system vibration caused by additional current. In addition, the rotor position can be directly detected by using a phase-locked loop (PLL) instead of using a low pass filter to get the EMF.

The expression of the hyperbolic tangent curve function is:

$$\begin{cases} s(x) = \dfrac{\exp(x) - \exp(-x)}{\exp(x) + \exp(-x)}, & x \neq 0 \\ s(x) = 0, & x = 0 \\ s(x) = 1, & x \to +\infty \\ s(x) = -1, & x \to -\infty \end{cases} \tag{13}$$

The image of the hyperbolic tangent function is shown in Figure 4.

The hyperbolic tangent function is used to replace the switching function, and the designed sliding mode control rate is:

$$\begin{bmatrix} v'_\alpha \\ v'_\alpha \end{bmatrix} = \begin{bmatrix} K_2 \tanh\left(i'_\alpha - i_\alpha\right) \\ K_2 \tanh\left(i'_\beta - i_\beta\right) \end{bmatrix} \tag{14}$$

Bring in the sliding mode control rate to obtain:

$$\begin{cases} \dfrac{\mathrm{d}\tilde{i}_\alpha}{\mathrm{d}t} = -\dfrac{R}{L_d}\,\tilde{i}_\alpha - (L_d - L_q)\,\omega_e \tilde{i}_\beta + \dfrac{1}{L_d}\left[E_\alpha - K_2 \tanh\left(i'_\alpha - i_\alpha\right)\right] \\ \dfrac{\mathrm{d}\tilde{i}_\beta}{\mathrm{d}t} = -\dfrac{R}{L_d}\,\tilde{i}_\beta + (L_d - L_q)\,\omega_e \tilde{i}_\alpha + \dfrac{1}{L_d}\left[E_\beta - K_2 \tanh\left(i'_\beta - i_\beta\right)\right] \end{cases} \tag{15}$$

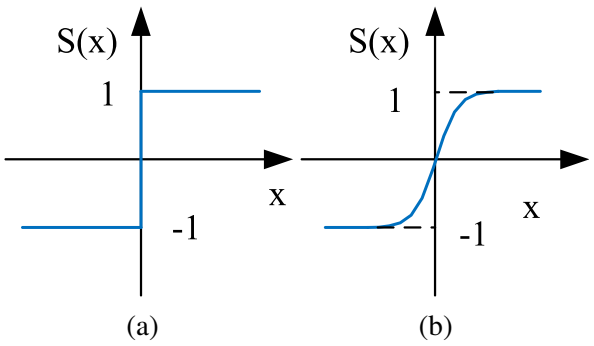

Figure 4. Comparison of switching function and hyperbolic tangent function.

When the sliding mode observer turntable variable approaches the sliding mode surface $i = 0$, the control variable can be obtained as:

$$\begin{bmatrix} E_\alpha \\ E_\beta \end{bmatrix} = \begin{bmatrix} v_\alpha \\ v_\beta \end{bmatrix} = \begin{bmatrix} K_2 \tanh\left(i'_\alpha - i_\alpha\right) \\ K_2 \tanh\left(i'_\beta - i_\beta\right) \end{bmatrix} \tag{16}$$

The sliding mode gain shall meet:

$$K_2 \geq \max\left\{-R\left|\tilde{i}_\alpha\right| + E_\alpha \tanh\left(\tilde{i}_\alpha\right), -R\left|\tilde{i}_\beta\right| + E_\beta \tanh\left(\tilde{i}_\beta\right)\right\} \tag{17}$$

Because the SMO is accompanied by high-frequency vibration and with the considering of the effect of the suspension force windings, this vibration is aggravated. Therefore, there will be high-frequency vibration in the estimated EMF. The rotor position estimation method based on the arctangent function directly introduces this vibration into the calculation, which causes the high frequency vibration to be amplified. This increases the angle estimation error.

Therefore, using PLL shown in Figure 5 to replace the arctangent function will effectively improve the accuracy of speed estimation.

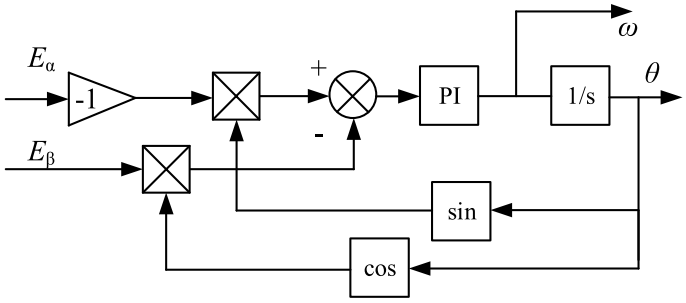

Figure 5. The realization block diagram of the PLL.

4.3. Simulation Verification

A special motor model is built in Matlab/Simulink. The suspension force windings is analogous to a special motor. This special motor system is equivalent suspension force windings to a motor running in asynchronous state. The speed of the equivalent asynchronous motor is the rotor speed, and the driving voltage is the suspension force winding voltage. In Figure 6, u_{aM}, u_{bM}, u_{cM} are the three phase driving voltages of torque windings; u_{aB}, u_{bB}, u_{cB} are the three phase driving voltages of suspension windings; T_{eM} is the torque generated by the torque windings; T'_e is the additional torque generated by suspension windings; i'_d, i'_q are the induced currents of suspension force magnetic field on torque windings.

$$T_e = (1-s)\frac{3}{2} P_B (L_{dB} - L_{qB}) i_{dB} i_{qB} \tag{18}$$

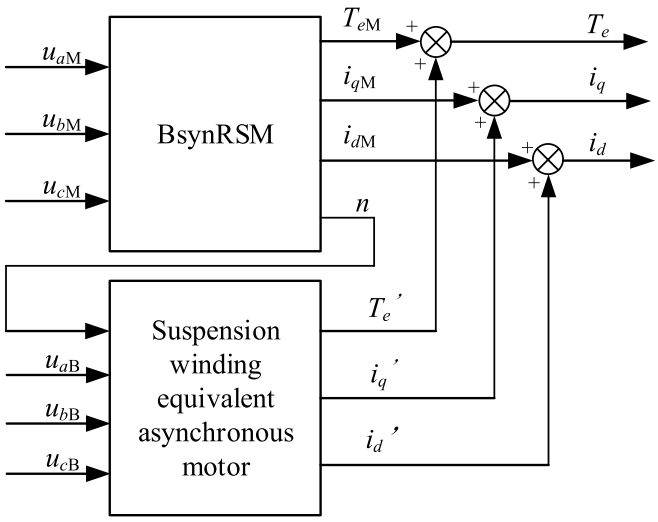

Figure 6. Model of BsynRSM considering the effect of suspension force winding.

where $s = (n_0 - n)/n$, n_0 is the synchronous speed of suspension windings.

When the motor starts, the rotor needs a strong magnetic field to move the rotor from the initial position to the center of the motor and achieve stable suspension. Therefore, the additional current caused by the suspension force windings during the startup process is relatively large. When the motor startup process is completed, the current required to overcome the rotor vibration will become the main part of the suspension force winding voltage. This part results in a sinusoidal oscillation of additional current and additional torque. Additional torque and additional current tend to be stable after 0.55 s. Due to the characteristics of the suspension force winding control system, if the suspension force winding voltage does not reach the limit value, the suspension force winding voltage will be proportional to the eccentric displacement of the rotor. It can be determined that the additional current and torque generated by the suspension force windings will be positively related to the rotor eccentric displacement. Therefore, in the Matlab/Simulink simulation model, the rotor displacement of the input force-current conversion module is doubled to verify the relationship between the rotor eccentric displacement and the additional current and additional torque.

Comparing Figure 7 and Figure 8, with the increase of rotor eccentric displacement, the additional current and additional torque generated by the suspension force windings increase approximately proportionally.

As the rotational speed increases, the eccentric displacement of the rotor does not increase significantly. Therefore, the additional current and torque generated by the suspension force windings

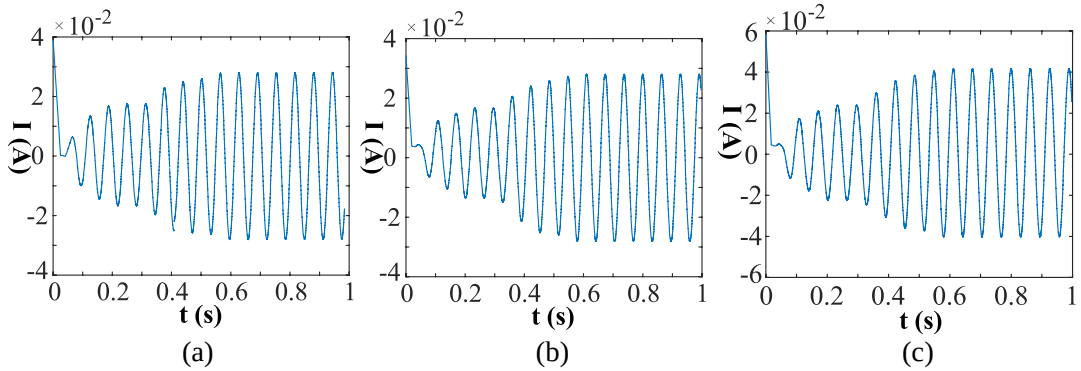

Figure 7. Additional current and torque caused by suspension force windings. (a) Additional i_d. (b) Additional i_q. (c) Additional torque.

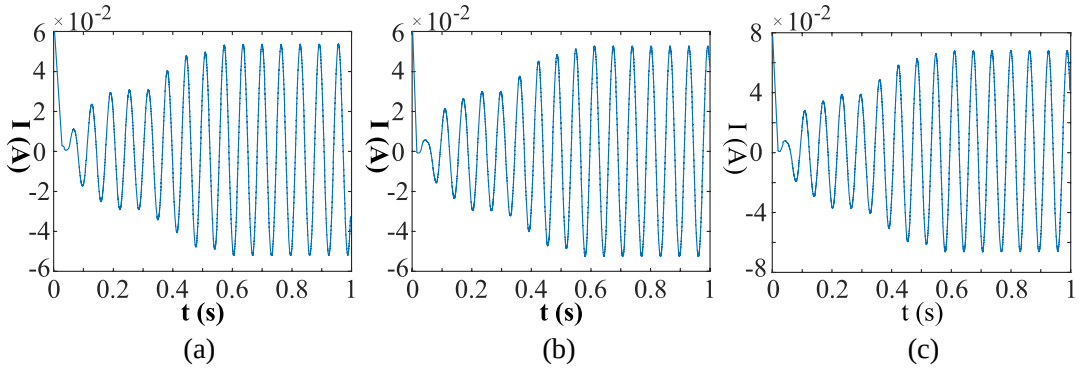

Figure 8. Additional current and torque caused by suspension force windings when the eccentric displacement of the rotor is doubled. (a) Additional i_d. (b) Additional i_q. (c) Additional torque.

hardly rise with the increase of the motor speed. However, as the motor speed increases, the EMF generated by the torque windings will increase, which will make the effect caused by additional current and torque generated by suspension force windings less obvious. So the BsynRSM is controlled at the speed of 1000 r/min. Since the vibration will stabilize with the additional current and torque, the simulation time is set to 0.8 s.

As shown in Figure 9, when the effect of suspension force windings is considered, the vibration amplitude of the speed estimation caused by the additional current generated by the suspension force windings is about 1.4 r/min. It is obvious that the vibration of the estimated speed increases, and the vibration has a certain periodicity. The amplitude of speed estimation vibration is not high, while this vibration will decrease the stability of the motor system, and this may increase the eccentric displacement of rotor.

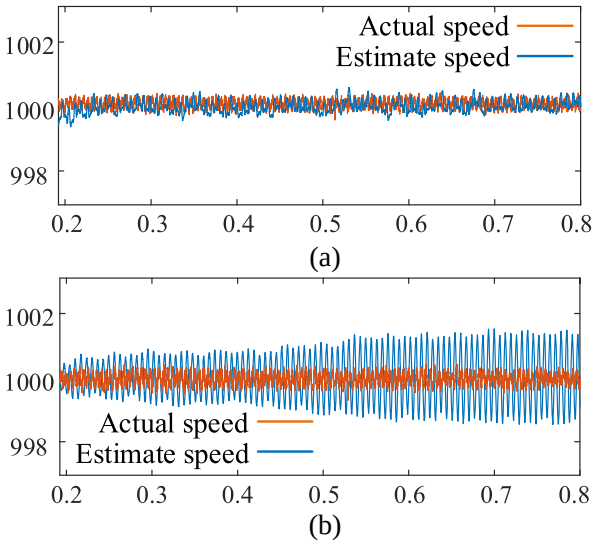

Figure 9. Comparison between actual speed and speed estimated by SMO after the motor runs stable. (a) When the effect of suspension force winding is not considered. (b) When the effect of suspension force winding is considered.

Also setting the given speed to 1000 r/min, the comparison between the estimated speed obtained by the improved SMO and the actual speed can be obtained. The estimated speed vibration obtained by the improved SMO is only 0.71 r/min, which is 49.3% lower than that of the traditional SMO, and the vibration frequency is significantly reduced. This will obviously improve the system stability. The results are shown in Figure 10.

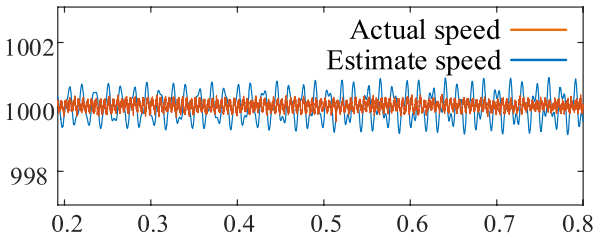

Figure 10. Comparison between actual speed and speed estimated by improved SMO after the motor runs stable.

5. EXPERIMENTAL VERIFICATION

In order to verify the above theoretical and simulated results, an experimental system is constructed as shown in Figure 11. In order to ensure the unity of experiment and simulation, the speed of BsynRSM experimental platform is set to 1000 r/min as the simulation. The SMO is constructed to estimate the rotor speed. On the experimental platform, as shown in Figure 12, the vibration caused by the suspension force windings is obviously greater than the Matlab/Simulink simulation. The amplitude of the vibration of the speed estimation when using the traditional SMO is about 17.2 r/min. When using the improved SMO, the amplitude of the vibration of the speed estimation is about 10.9 r/min. The amplitude of speed estimation vibration when using improved SMO is 36.6% less than that when using the traditional SMO. And the frequency is much lower. The experiment verifies the effect of the suspension force windings on the speed sensorless control, and the improved SMO effectively reduces the amplitude and frequency of speed estimation vibration.

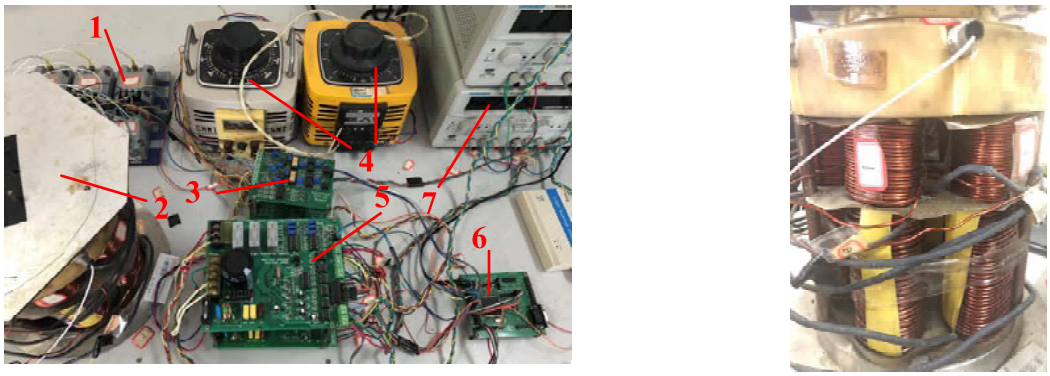

(a) (b)

Figure 11. BsynRSM experimental platform. (a) 1. Eddy current sensor. 2. Fixing plate of Hall sensor. 3. Interface circuit. 4. Transformer. 5. Driving circuit. 6. DSP circuit. 7. DC voltage source. (b) BsynRSM.

When the motor is accelerated to the rated speed of 3000 r/min, the estimated speed accuracy obtained by the SMO is slightly improved due to the increase of the EMF of the motor. However, as the rotational speed increases, the vibration frequency of the rotor also increases significantly. Therefore, the voltage frequency of the suspension force winding increases accordingly, resulting in an increase in the vibration frequency of the speed estimation error of the SMO. As shown in Figure 13, the amplitude of the estimated speed has a certain decrease to 15.8 r/min, while the frequency has obviously increased. After using the improved SMO, the vibration amplitude of the rotational speed estimation also decreases by 35.4% to 10.2 r/min, and the vibration frequency has a certain reduction. Therefore, it can be considered that the improved SMO can effectively improve the performance of speed estimation and the stability of the system under various operating states of the motor.

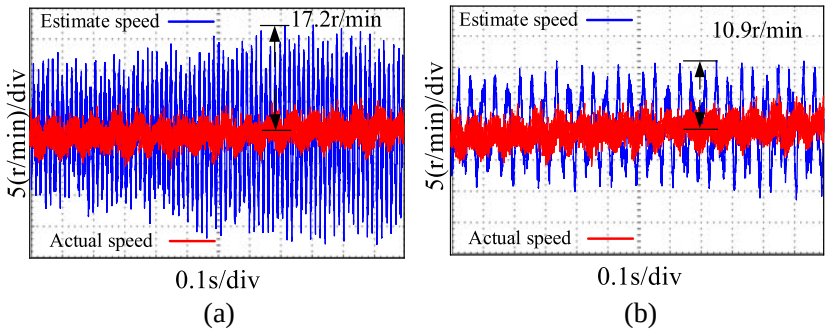

Figure 12. Comparison between measured actual speed and estimated speed after speed stabilization when the speed is 1000 r/min. (a) When using traditional SMO. (b) When using improved SMO.

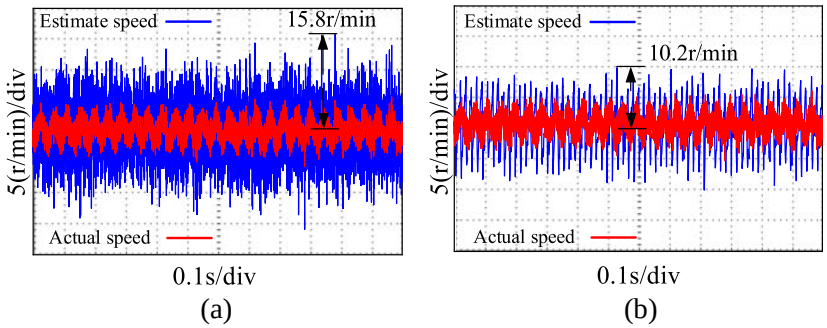

Figure 13. Comparison between measured actual speed and estimated speed after speed stabilization when the speed is 3000 r/min. (a) When using traditional SMO. (b) When using improved.

6. RESULTS AND DISCUSSION

For the BsynRSM, due to the characteristics of the slice motor, its axial suspension is passive. So only the radial suspension force needs to be controlled to ensure the rotor at the center position. The driving voltage required for the suspension force windings is proportional to the rotor eccentric displacement. Therefore, the additional current and torque caused by the suspension force windings will be related to the unbalanced vibration of the rotor. When the motor starts, the suspension force windings need a larger voltage to establish the suspension magnetic field, so the additional current and torque are larger. This may lead to a large error in the speed estimation at startup. With the stable suspension of the motor, the driving voltage of the suspension force windings drops quickly. However, the additional current generated by the suspension force windings still has a large impact on the speed sensorless control based on the SMO. This results in a high frequency sinusoidal vibration in the speed estimation. This vibration will greatly reduce the stability of the motor system and further increase the eccentric displacement of the rotor. By using the improved SMO proposed in this paper, the vibration amplitude of rotational speed estimation is effectively reduced, and the vibration frequency of rotational speed estimation is limited to a lower level. This improved SMO effectively improves the stability of the system operation.

In order to further reduce the effect of the suspension force windings, the following methods can be used:

1. When running a sensorless system, minimize the use of motor torque and winding current.
2. Reduce the vibration of the rotor. By introducing the rotor vibration compensation strategy and other methods, reduce the amplitude of the rotor vibration. Then the driving voltage of the suspension force windings will be reduced, so the additional torque and additional current caused by the suspension force windings will be reduced. Finally, the effect on sensorless system will be reduced.

3. Due to the inertia of the rotor, the frequency of motor speed change is lower than the frequency of rotor vibration. So, speed change is also lower than the frequency of additional current and additional torque caused by the suspension force windings. Therefore, the influence of the suspension force windings can be reduced by limiting the high-frequency part of the motor speed estimated.

7. CONCLUSIONS

Through the establishment of Maxwell simulation model, this paper finds the effect of suspension force windings on the torque windings in a BsynRSM based on the conclusion of BsynRM. Suspension force windings will cause additional current in the torque windings and generate additional asynchronous torque. Additional current and torque will cause a sinusoidal vibration for the speed sensorless estimation, and the frequency of speed estimation vibration is much higher than the additional current and torque. This high frequency vibration will reduce the stability of motor system. An improved SMO is proposed in this paper. By using the hyperbolic tangent curve instead of the switching function and using PLL instead of the arctangent function, the frequency of the speed estimation vibration is significantly reduced. The amplitude of speed estimation vibration is reduced 36.6% when the speed of the motor is 1000 r/min, and the speed estimation vibration is reduced 35.4% when the speed of the motor is 3000 r/min. In future work, the effects of additional current and torque generate by suspension force windings on other speed sensors will be further analyzed, and schemes to reduce these effects will be designed.

ACKNOWLEDGMENT

This project was sponsored in part by the National Natural Science Foundation of China (61973144, 62273168).

REFERENCES

1. Sun, X., L. Chen, and Z. Yang, "Overview of bearingless permanent-magnet synchronous motors," *IEEE Transactions on Industrial Electronics*, Vol. 60, No. 12, 5528–5538, 2013.
2. Sawada, M., et al., "A study on a bearingless drive of a surface permanent magnet synchronous motor," *15th International Conference on Electrical Machines and Systems*, 1–4, Sapporo, Japan, 2012.
3. Steinert, D., T. Nussbaumer, and J. Kolar, "Slotless bearingless disk drive for high-speed and high-purity applications," *IEEE Transactions on Industrial Electronics*, Vol. 61, No. 11, 5974–5986, 2014.
4. Puentener, P., M. Schuck, J. W. Kolar, and D. Steinert, "Comparison of bearingless slice motor topologies for pump applications," *2019 IEEE International Electric Machines & Drives Conference*, 9–16, Santiago, Chile, 2019.
5. Gruber, W., "Bearingless slice motors: General overview and the special case of novel magnet-free rotors," *Innovative Small Drives and Micro-Motor Systems*, 1–6, Nuremberg, Germany, 2013.
6. Takemoto, M., K. Yoshida, N. Itasaka, Y. Tanaka, A. Chiba, and T. Fukao, "Synchronous reluctance type bearingless motors with multi-flux barriers," *2007 Power Conversion Conference*, 1559–1564, Nagoya, Japan, 2007.
7. Mukherjee, V., J. Pippuri, S. E. Saarakkala, A. Belahcen, M. Hinkkanen, and K. Tammi, "Finite element analysis for bearingless operation of a multi flux barrier synchronous reluctance motor," *18th International Conference on Electrical Machines and Systems*, 688–691, Pattaya, Thailand, 2015.
8. Ding, H., H. Zhu, and Y. Hua, "Optimization design of bearingless synchronous reluctance motor," *IEEE Transactions on Applied Superconductivity*, Vol. 28, No. 3, 1–5, April 2018.
9. Mukherjee, V., P. Rasilo, F. Martin, and A. Belahcen, "Analysis of electromagnetic force ripple in a bearingless synchronous reluctance motor," *IEEE Transactions on Magnetics*, Vol. 57, No. 2, 1–8, 2021.

10. Diao, X., H. Zhu, Y. Qin, and Y. Hua, "Torque ripple minimization for bearingless synchronous reluctance motor," *IEEE Transactions on Applied Superconductivity*, Vol. 28, No. 3, 1–5, April 2018.
11. Holenstein, T., T. Nussbaumer, and J. W. Kolar, "A bearingless synchronous reluctance slice motor with rotor flux barriers," *2018 International Power Electronics Conference*, 3619–3626, Niigata, Japan, 2018.
12. Sokolov, M., W. Gruber, S. E. Saarakkala, and M. Hinkkanen, "Modeling of a bearingless synchronous reluctance motor with combined windings," *2019 IEEE Energy Conversion Congress and Exposition*, 7084–7090, Baltimore, Maryland, USA, 2019.
13. Holenstein, T., M. Schuck, and J. W. Kolar, "Performance benchmarking of a novel magnet-free bearingless synchronous reluctance slice motor," *IEEE Open Journal of the Industrial Electronics Society*, Vol. 1, 184–193, 2020.
14. Chiba, A., K. Chiba, and T. Fukao, "Principles and characteristics of a reluctance motor with windings of magnetic bearing," *Proc. of IPEC*, 919–926, Tokyo, 1990.
15. Belahcen, A., V. Mukhrejee, F. Martin, and P. Rasilo, "Computation of hysteresis torque and losses in a bearingless synchronous reluctance machine," *IEEE Transactions on Magnetics*, Vol. 54, No. 3, 1–4, 2018.
16. Li, P., L. Zhang, and Y. Yu, "A novel sensorless for switched reluctance motor based on sliding mode observer," *IEEE 2nd Advanced Information Technology, Electronic and Automation Control Conference*, 1560–1564, Chongqing, China, 2017.
17. Foo, G. H. B. and M. F. Rahman, "Direct torque control of an IPM-synchronous motor drive at very low speed using a sliding-mode stator flux observer," *IEEE Transactions on Power Electronics*, Vol. 25, No. 4, 933–942, 2010.